Int. J. Electrochem. Sci., 11 **(2016)** 710 - 723

International Journal of
ELECTROCHEMICAL
SCIENCE
www.electrochemsci.org

Anodization of Highly Ordered TiO_2 Nanotube Arrays Using Orthogonal Design and Its Wettability

Jiangxue Wang[*], *Hui Li, Yang Sun, Bing Bai, Yaohua Zhang, Yubo Fan*[*]

Key Laboratory for Biomechanics and Mechanobiology of Ministry of Education; School of Biological Science and Medical Engineering, Beihang University, Beijing, 100191, China
[*]E-mail: wangjiangxue@buaa.edu.cn, yubofan@buaa.edu.cn

Received: 31 October 2015 / *Accepted:* 20 November 2015 / *Published:* 1 December 2015

Using orthogonal design of experiments (DOE), the highly ordered TiO_2 nanotube arrays on Ti6Al4V alloy was achieved by anodic oxidation in a standard two-electrode system. According to the $L_{16}(4^5)$ orthogonal array, sixteen experimental runs were set for anodizing voltage, duration time and H_2O content in the electrolyte with four different levels. Scanning electron microcopy (SEM) images showed the various features of TiO_2 nanotubes anodized at different electrochemical conditions. The long neat nanotube with honeycomb-like structure was also formed in an array. The range analysis and variance analysis of DOE revealed that the voltage was the primary factor to influence the dimension of the anodized TiO_2 nanotubes. The sequence of influential factors was voltage > duration time > H_2O content. The optimal level for the H_2O content and duration time was 4 wt% and 3h, respectively. The surface wettability of Ti6Al4V alloy became hydrophilic and enhanced with the anodizing voltage increasing.

Keywords: anodization; TiO_2 nanotube arrays; orthogonal design; anodizing voltage; duration time; H_2O content

1. INTRODUCTION

Compared with the common surface of materials, arrays of TiO_2 nanotubes formed by anodization have gained much concern in last decade because of its nano-array feature on Ti or Ti alloy. The remarkable nano-characteristic is potentially promising in a wide field of application, including dye-sensitized solar cells [1], water splitting [2], drug delivery [3], and biomedical implants [4, 5]. Ti6Al4V alloy is successfully used in medical prosthesis and orthopedic and dental implants from the 1950s, owing to its plasticity, toughness, strength, weldability, corrosion resistance and biocompatibility. The implants failure generally occurs between the implant and the underlying bone surface because of poor osseointegration, though a thin layer of passive and protective natural TiO_2 is formed on the surface. For enhancing the interaction between orthopedic implant and bone, the anodization of TiO_2 nanotube arrays on Ti alloy is a simple and practicable way to improve cell adhesion and to accelerate bone growth [6-8].

The growth of nanoporous TiO_2 film on Ti and Ti6Al4V alloy is firstly reported by Zwilling et al. in chromic acid media containing HF [9]. It is well known that TiO_2 nanotube arrays can grow up in two kinds of electrolyte, one is aqueous-based electrolyte, and the other is organic-based electrolyte. The fluoride ion in the electrolyte is necessary for the fabrication of the nanostructure on Ti and its alloys [10-12]. Using Ti or Ti alloy as anode, Pb as cathode, Gong et al. successfully fabricated the TiO_2 nanotubes in aqueous electrolyte containing HF [13]. However, in these early works, the tube length was of only few hundred nanometers with a relatively low degree of order. Since then, many researchers devoted to the anodization method to seeking for how to tune the morphology of TiO_2 nanotubes.

The geometric characteristics of nanotube arrays are determined by multiple factors, including anodizing voltage, duration time, temperature, electrolyte composition (including organic- or water-based electrolyte, pH, and water content) and its viscosity [7, 14, 15]. By tailoring the electrochemical parameters and the electrolyte concentration, Macak et al. achieved TiO_2 nanotubes with high aspect ratio in organic electrolyte [16]. The length of nanotubes can be controlled precisely from several to hundreds of micrometers when the organic-based electrolyte is used, such as ethylene glycol. In the past decades, both the field-assisted dissolution model and the “plastic flow” model are elaborated to illustrate the growth mechanism of nanotubes in fluoride-containing electrolytes [7, 10, 17-19]. In 2008, Zhu et al. introduced a growth model of oxygen bubble mould (OBM), which emphasizes that the oxygen bubble is the precondition of the oxide flow from the pore base to the pore wall [20, 21]. Until now, the mechanism is still in controversial and unclear. However, it is well known that the anodizing voltage, duration time and water content in electrolyte are important factors in the process of nanotube growth. To fabricate the highly ordered TiO_2 nanotube arrays on Ti or Ti alloy for further bone application, it is difficult to select the electrochemical conditions and to determine the electrolyte composition. The aim of this paper is to provide a systematic approach to grow highly-organized TiO_2 nanotube arrays on Ti6Al4V alloy by orthogonal design of experiments (DOE). The morphology of nanotube arrays is analyzed by scanning electron microscopy, and the surface wettability is measured by a contact angle meter.

2. MATERIAL AND METHODS

2.1 Materials

Ti6Al4V alloy (1mm thickness) was purchased from Chang’an Minglong Mould Steel (Dongguan, Guangdong). The samples of Ti alloy (10×10×1mm) were cut, and then mechanically polished with silicon carbide sandpaper of 400, 800, 1200 and 2000 grits successively. The surface of each sample was washed with acetone, ethanol and distilled water by ultrasonic for 15 min. NH_4F and acetone were obtained from Beijing Chemical Works (Beijing), and ethylene glycol (EG) and absolute ethanol were obtained from Guangfu Fine Chemical Research Institute (Tianjin). All chemicals used in this study were of AR grade.

2.2 Orthogonal design of experiments

For experimental design, parameter optimization is a significant step to obtain a highly ordered TiO_2 nanotube arrays on Ti6Al4V alloy. In this study, the method of orthogonal experimental design was used. The different levels for anodizing voltage, duration time and H_2O content in the electrolyte were selected and listed in Table 1. According to the $L_{16}(4^5)$ orthogonal array, 16 experimental runs were set and shown in Table 2.

Table 1. Levels for anodizing voltage, time and H_2O content in the orthogonal experimental design

Levels	Factors		
	Voltage (V) A	H_2O content (wt%) B	Duration Time (h) C
I	20	2	2
II	30	3	3
III	40	4	4
IV	50	5	5

Table 2. Experimental runs in the orthogonal design using $L_{16}(4^5)$ orthogonal array

Experimental runs	Sample No.	Voltage (V)	H_2O content (wt%)	Duration time (h)
1	S1	AI	BI	CI
2	S2	AI	BII	CII
3	S3	AI	BIII	CIII
4	S4	AI	BIV	CIV
5	S5	AII	BI	CII
6	S6	AII	BII	CI
7	S7	AII	BIII	CIV
8	S8	AII	BIV	CIII
9	S9	AIII	BI	CIII
10	S10	AIII	BII	CIV
11	S11	AIII	BIII	CI
12	S12	AIII	BIV	CII
13	S13	AIV	BI	CIV
14	S14	AIV	BII	CIII
15	S15	AIV	BIII	CII
16	S16	AIV	BIV	CI

According to the H_2O content (table 1), the electrolyte was prepared by mixing EG, H_2O and 0.25 wt% NH_4F in a glass beaker at room temperature (about 25°C). Based on 16 experimental runs listed in table 2, the anodization was performed in a two-electrode system with Ti alloy as the anode and plumbum foil as the cathode under an anodizing voltage supplied by a DH1720A-4 DC power source (60V1A, Dahua Electronic, Beijing, China). The distance between the two electrodes is kept at 3 cm in all anodizing process. After electrochemical anodization, the as-anodized TiO_2 nanotube arrays was rinsed with deionized water and then ultrasonicated in ethanol for 1 min.

2.3 TiO_2 nanotubes fabricated at different anodizing voltage

To detect the influence of anodizing voltage on the morphology of nanotube, the voltage gradient (including 20, 25, 30, 35, 40, 45, 50, 55, and 60 V) was performed to fabricate TiO_2 nanotubes in the electrolyte mixed with EG, 0.25 wt% NH_4F and 3 wt% H_2O for 3 h.

2.4. Characterization of TiO_2 nanotube arrays

The morphology of the TiO_2 nanotube arrays on Ti6Al4V was observed using field emission scanning electron microscope (QUANTA FEG250, FEI) at an accelerating voltage of 20 kV. Finally, the dimensions of TiO_2 nanotubes were measured using ImageJ software (NIH, USA). The mean and standard deviation (SD) were used to measure the dispersion of nanotubes.

The static water contact angle measurements of the TiO_2 nanotube arrays were carried out on a JY-82C contact angle analyzer (Chengde, China) to quantify the degree of hydrophilia. The scan area was 10 mm ×10 mm.

2.5 Statistical analysis

All data about the diameter of nanotubes was statistically analyzed using SPSS 13.0 for windows (SPSS Inc., Chicago, IL, USA). The range analysis and variance analysis were carried out for the orthogonal experimental design. $P < 0.05$ was set as the statistically significant.

3. RESULTS AND DISCUSSION

3.1 Morphology of TiO_2 nanotube arrays growth in fluoride-containing EG electrolytes

Figure 1 shows the SEM images of the TiO_2 nanotube arrays anodized at 20V using the orthogonal design of experimental method. In Figure 1a, the small nanopores have been grown on the surface of Ti6Al4V at 20V, 2.0 wt% H_2O for 2h. The porous layer partially covers on the nanotubes (Figure 1a and 1b). This is initiated during the first stage of growth, also called compact oxide layer [22]. The porous layer is absent on the nanotubes fabricated under other conditions. From the sectional view (inset of Figure 1), it is clear that the nanotubes are long, and the close-packed clusters of nanotube are formed at the top parts of the tubes, which is called nanograss. .

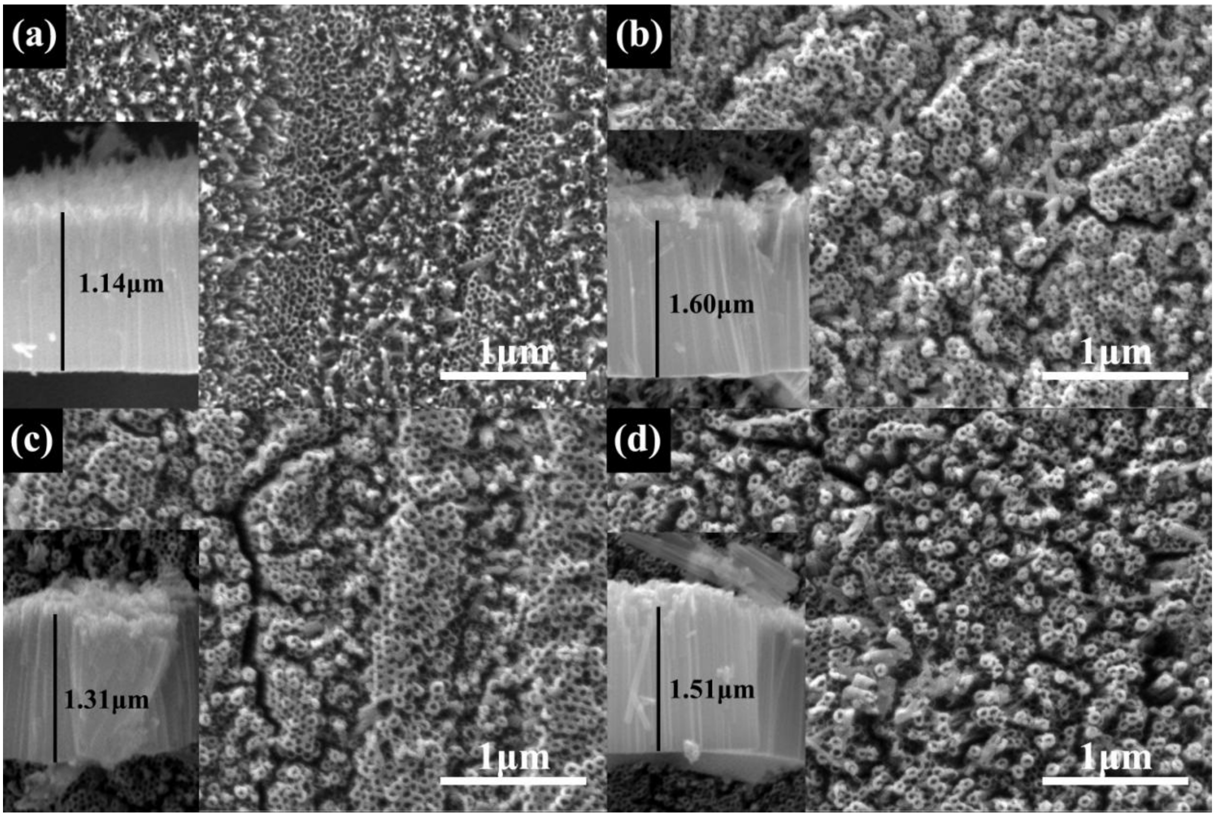

Figure 1. SEM images of TiO_2 nanotube arrays fabricated by anodization at 20V using orthogonal experimental design. (a) S1, (b) S2, (C) S3, (d) S4

In an electrochemical cell, anodization of a metal is a self-organized process to create porous or tubular oxide layer on metal substrate (anode or working electrode) with an inert counter electrode (usually platinum, carbon or plumbum). For aluminium, hexagonal nanoporous alumina is usually formed in fluoride-containing electrolytes. For Ti or Ti alloys, at an applied voltage, Ti^{4+} ions are driven from Ti substrate toward the electrolyte and a compact TiO_2 oxide layer grows initially on the anode surface because the water is electrolyzed to cause the field-assisted movement of ions (Eq. 1&2). Then, in the fluoride-containing electrolyte, the field-assisted dissolution at the metal-oxide interface (Eq 3) and chemical dissolution at the oxide-electrolyte interface (Eq. 4) are followed simultaneously to form tubular layer. It is shown as the following:

Metal oxidation: $Ti \text{ ----> } Ti^{4+} + 4e^-$ (Eq. 1)

Oxide layer formation: $Ti + 2H_2O \text{ ---> } TiO_2 + 4H^+$ (Eq. 2)

Field-assisted dissolution: $Ti^{4+} + 6F^- \text{ ----> } [TiF_6]^{2-}$ (Eq. 3)

Chemical dissolution: $TiO_2 + 6F^- + 4H^+ \text{ ----> } [TiF_6]^{2-} + 2H_2O$ (Eq. 4)

When the oxide growth at the metal-oxide interface under high field condition balances with the dissolution at the oxide-electrolyte interface, the steady state is reached, leading to the self-ordering nanotube growth, at the same time, the thickness of nanotubular layer remains unchanged.

According to the process of anodization, the applied voltage, duration time, and water content in electrolyte are the key factors when fabricating TiO_2 nanotubes. In organic electrolyte containing EG, the long nanotubes with high aspect ratio are generally obtained. However, with the duration time extended, the top part of ordered long nanotubes disintegrated and transformed into nanograss. The formation mechanism of nanograss was fully elaborated because the nanotubes were bundled on the top surface of TiO_2-nanotubes [23-25]. The bundling of nanotubes is mainly induced by the over-etching of the top parts that are very thin and fragile [26]. Lee et al. [17] reported that the chemical etching thinned out and finally penetrated tube walls, resulting in some needle-like structures at the tube tops and collapse. Apart from the duration time, the morphology of nanotubes depends on the amount of H_2O in the electrolyte. The 8 % water content could result in the "ripples" on the wall of the nanotubes.

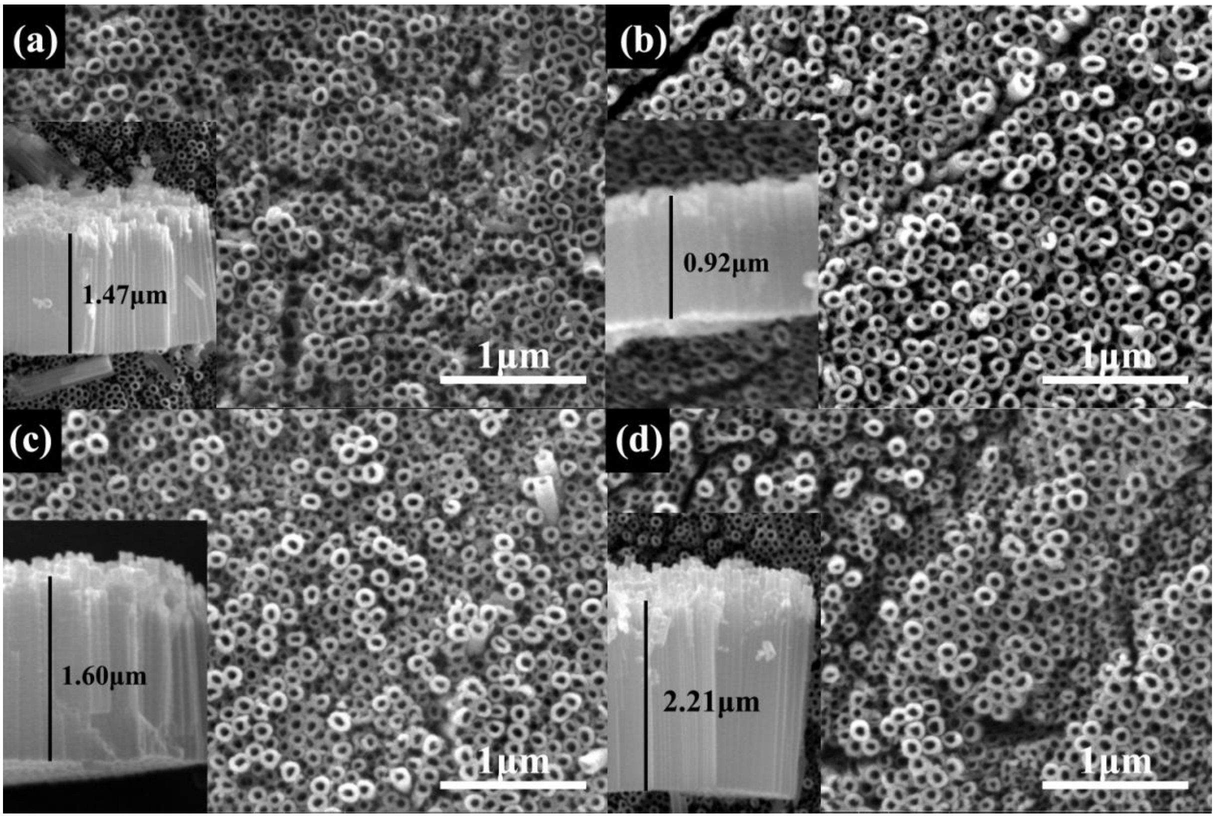

Figure 2. SEM images of TiO_2 nanotube arrays fabricated by anodization at 30V using orthogonal experimental design. (a) S5, (b) S6, (C) S7, (d) S8

Thus, to obtain the highly ordered arrays, the H_2O content is limited in the organic electrolyte. In this study, the different H_2O content is selected including 2 wt%, 3 wt%, 4 wt%, and 5 wt%. Figure 2 is the SEM images of TiO_2 nanotube arrays anodized at 30V. The comparatively neat TiO_2 nanotube arrays is formed on the surface of Ti6Al4V alloy. With the increase of H_2O content from 2 wt% to 5 wt%, the neat and distinct TiO_2 nanotube is anodized with the clear surface. At the same time, the ripples are observed on the tube wall from the inset sectional view of Figure 2c-d, but not found on the tube wall of Figure 2a. It is reported that the ribs at the tube wall are closely correlated with the water content in the electrolyte [27, 28]. No water-containing organic electrolyte result in very smooth nanotube without ripples. Berger et al. [28] studied the influence of 0-50 vol% water content in EG electrolyte on the morphology change of anodic TiO_2. They observed that the ribs were formed at the side wall of aligned nanotubes at 2.5 vol% or higher water content. The reasonable formation mechanism of ripples was illustrated according to the different mechanism [10, 27]. Based on the filed-assisted dissolution mechanism, the formation of ribs is ascribed to the continuous etching and passivation of the cell boundary regions (a faster chemical dissolution speed than the growth speed of the tubes). However, Chong et al. set a series of experiments to prove that the ribs on the external tube walls resulted from the electrolyte entering into the wider gaps among the nanotubes due to the rupture of the entire surface layer by combining the 'plastic flow' model and the oxygen bubble model [21].

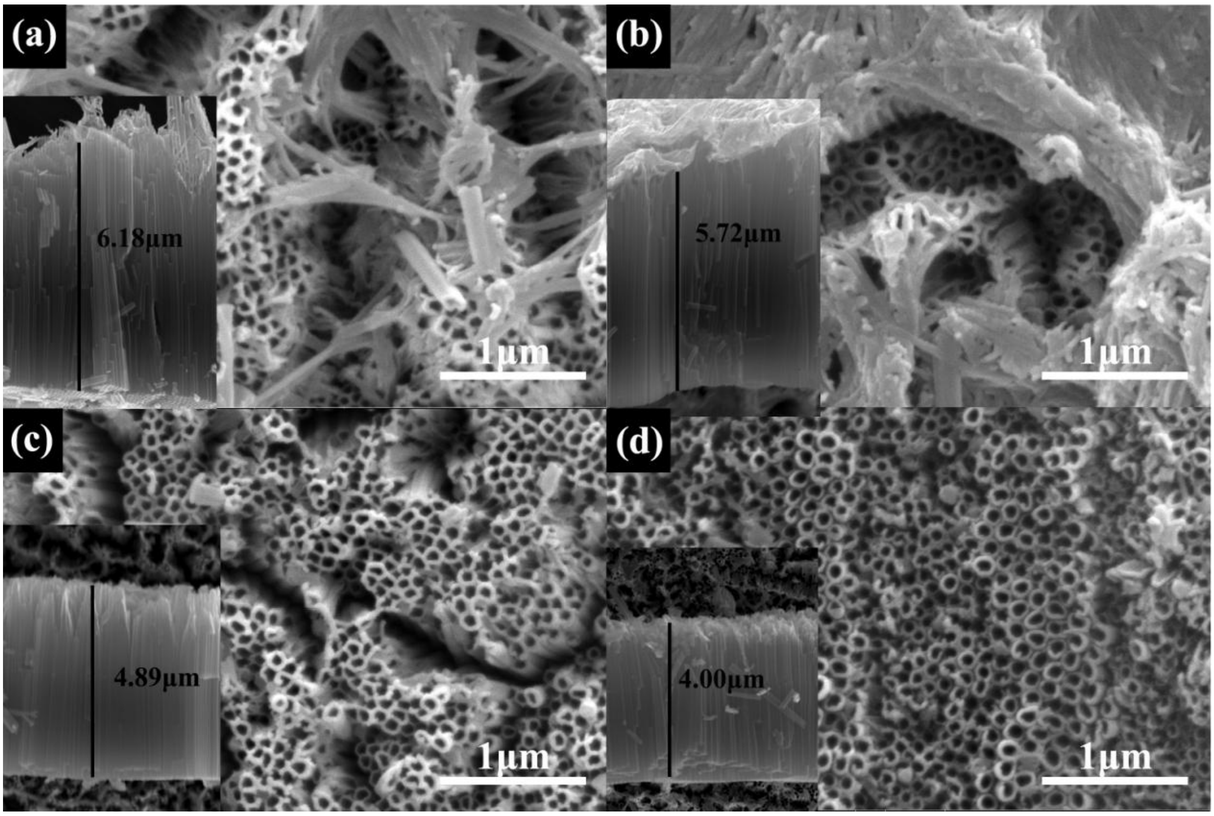

Figure 3. SEM images of TiO_2 nanotube arrays fabricated by anodization at 40V using orthogonal experimental design. (a) S9, (b) S10, (C) S11, (d) S12

Figure 3 is the SEM images of TiO_2 nanotube arrays anodized at 40V. The well-defined tubular structure is not shown under these conditions. The serous collapse and disintegrate of the top part of TiO_2 nanotubes are formed in EG electrolyte with 2 wt% H_2O for 4h and with 3 wt% H_2O for 5h, which are shown in Figure 3a and 3b, respectively. Though the collapse of nanotube is not occurred in EG electrolyte with 4 wt% H_2O for 2h (Figure 3C) and with 5 wt% for 3h (Figure 3D), the cluster of nanotubes and nanograss are viewed from the sectional view of Figure 3C and 3D (insets).

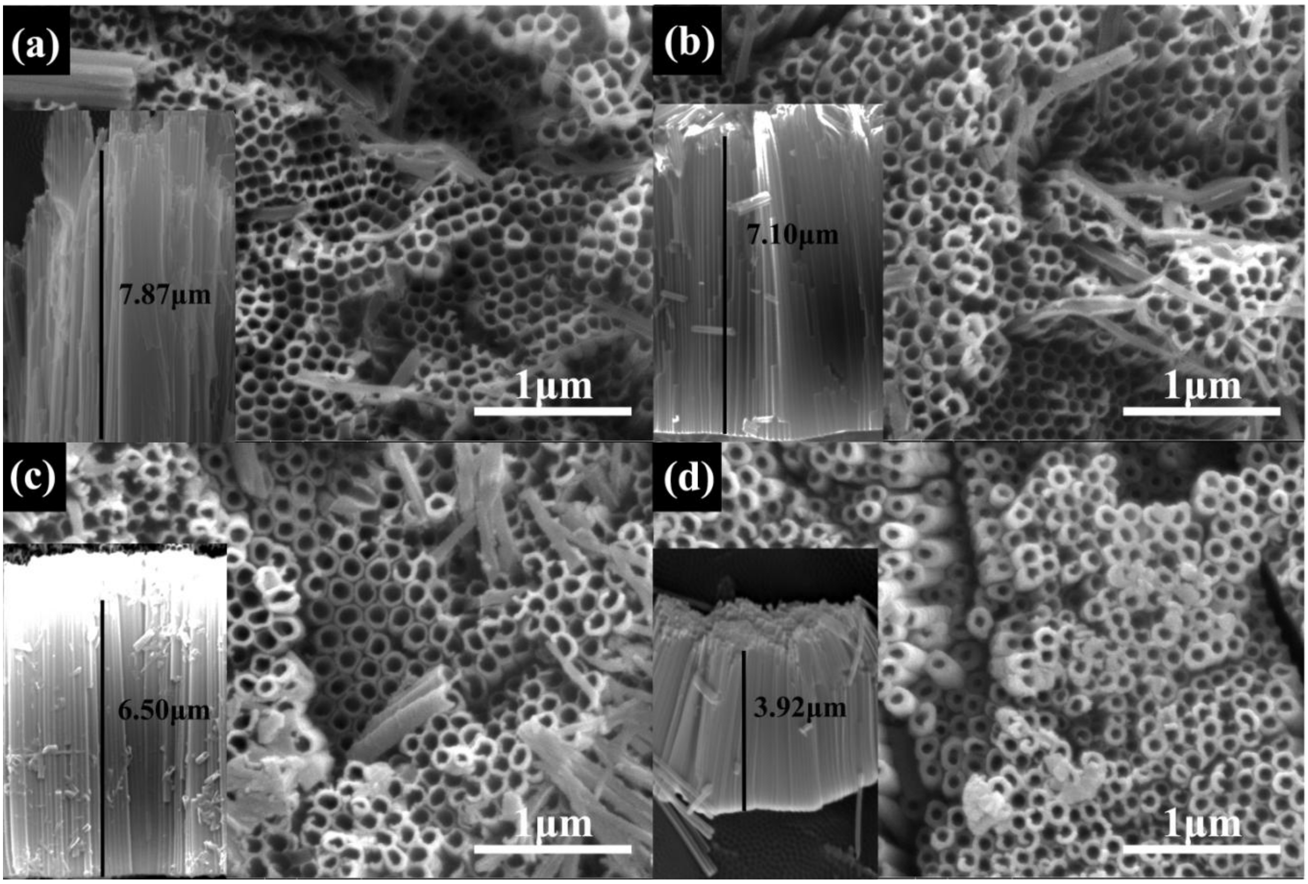

Figure 4. SEM images of TiO_2 nanotube arrays fabricated by anodization at 50V using orthogonal experimental design. (a) S13, (b) S14, (C) S15, (d) S16

Figure 4 is the SEM images of nanotube arrays anodized at 50V. The large diameter and the long neat nanotubes are formed. This is in line with earlier report that the anodizing voltage controls the tube diameter [29]. The tube length is adjusted by the duration time [30]. Generally, the nanotube is single and arranges in an array. However, the honeycomb-like tubular structure is occurred in the images of Figure 3a, c and Figure 4a, b. The wall of tube is thinned down, and it is too brittle and easy to crack.

The mean and standard deviation (SD) of the diameter for the anodized TiO_2 nanotubes are listed in Table 3. The orthogonal experimental design is to estimate the main effects and interaction independently in an orthogonal manner with a minimum number of runs in the experiment. The range analysis of orthogonal experimental design for the mean diameter of the anodized nanotubes is shown in Table 4a. From the range R, it is obvious that the voltage is the primary factor to influence the diameter size of the anodized nanotubes. The sequence of influential factors is voltage > duration time > H_2O content. The variance analysis of orthogonal experimental design for the mean diameter is analyzed using SPSS software, which is listed in Table 5a. The statistical significant difference is only existed for the voltage ($p < 0.05$), which is consistent with the result of range analysis. Further, the TiO_2 nanotube is anodized at different voltage. The diameter of anodized TiO_2 nanotubes is linear with the anodizing voltage, which is shown in Figure 6. The correlation coefficient R is 0.99.

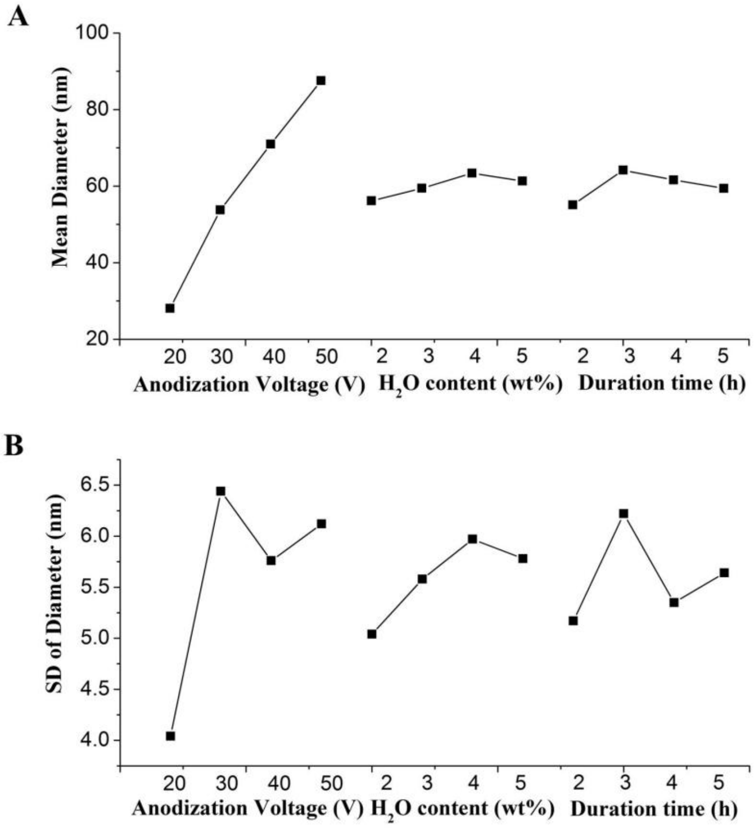

Figure 5. The trend diagram of each factor on the mean (A) and SD (B) of nanotubes diameter

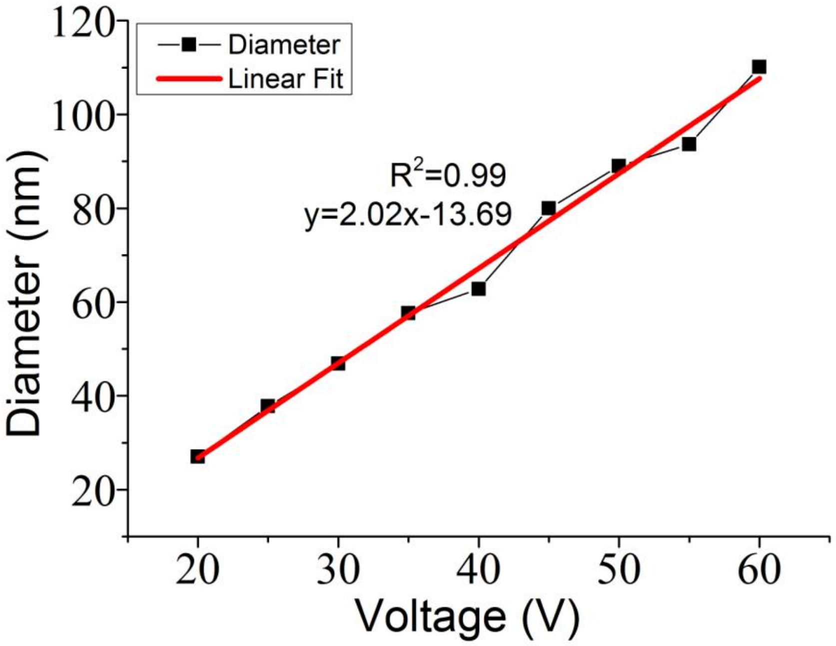

Figure 6. Linear correlation of the mean diameter of nanotubes with the anodizing voltage

Table 4b and 5b show the range analysis and variance analysis for the SD of the diameter for the anodized nanotubes. The range analysis indicates that the optimal factor affecting the SD of diameter is the voltage, and then is the duration time, and the minor factor is the water content. The influential sequence is voltage > duration time > H_2O content, which is consistent with that of the mean diameter. This result shows that the anodizing voltage is the first and most important factor in the process of TiO_2 anodization. The voltage not only is linearly correlated with the tubes diameter, but also closely determines the uniformity of anodized nanotubes though the significance is not existed (F=1.856, *p*=0.238, Table 5b). The trend diagram of each factor (Figure 5) indicates that the optimal level of the water content and duration time is 4 wt% and 3h, respectively.

Table 3. The mean and standard deviation (SD) of diameter for anodized TiO_2 nanotubes using orthogonal experimental design

Sample No.	Voltage (V)	H_2O content (wt%)	Duration time (h)	Mean Diameter (nm)	SD of Diameter (nm)
S1	20	2	2	25.5	5.0
S2	20	3	3	27.8	4.1
S3	20	4	4	32.4	2.9
S4	20	5	5	26.5	4.2
S5	30	2	3	49.1	6.3
S6	30	3	2	50.4	4.9
S7	30	4	5	53.8	7.1
S8	30	5	4	61.8	7.4
S9	40	2	4	68.8	4.7
S10	40	3	5	76.1	7.0
S11	40	4	2	63.3	5.3
S12	40	5	3	75.7	6.0
S13	50	2	5	81.3	4.2
S14	50	3	4	83.5	6.4
S15	50	4	3	104.1	8.5
S16	50	5	2	81.3	5.4

Table 4a. Range analysis of orthogonal experimental design for the mean diameter of the anodized nanotubes

Levels	Anodizing voltage (V)	H_2O content (wt%)	Duration time (h)
Ⅰ	28.0	56.2	55.1
Ⅱ	53.8	59.5	64.2
Ⅲ	71.0	63.4	61.6
Ⅳ	87.6	61.3	59.4
Range (R)	59.5	7.2	9.0
Optimal factor	Voltage > Time > H_2O content		

Table 4b. Range analysis of orthogonal experimental design for the standand deviation (SD) of diameter of the anodized nanotubes

Levels	Anodizing voltage (V)	H_2O content (wt%)	Duration time (h)
Ⅰ	4.04	5.04	5.17
Ⅱ	6.44	5.58	6.22
Ⅲ	5.76	5.97	5.35
Ⅳ	6.12	5.78	5.64
Range (R)	2.40	0.93	1.05
Optimal factor	Voltage > Time > H_2O content		

Table 5a. Variance analysis of orthogonal experimental design for the mean diameter of the anodized TiO_2 nanotubes

Source	Sum of Squares	df	Mean Square	F	Sig.
Corrected Model[a]	8045.323	9	893.925	16.932	0.001
Intercept	57768.123	1	57768.123	1094180	0.000
Voltage	7755.903	3	2585.301	48.968**	0.000
H_2O content	112.873	3	37.624	0.713	0.579
Duration Time	176.548	3	58.849	1.115	0.414
Error	316.775	6	52.796		
Total	66130.220	16			
Corrected Total	8362.098	15			

a: R Square=0.962 (Adjusted R Square=0.905)

Table 5b. Variance analysis of orthogonal experimental design for the standard deviation of diameter of the anodized nanotubes

Source	Sum of Squares	df	Mean Square	F	Sig.
Corrected Model[a]	18.162	9	2.018	0.820	0.621
Intercept	500.305	1	50.305	203.400	0.000
Voltage	13.694	3	4.565	1.856	0.238
H_2O content	1.918	3	0.639	0.260	0.852
Duration Time	2.550	3	0.850	0.346	0.794
Error	14.758	6	2.460		
Total	533.226	16			
Corrected Total	32.920	15			

3.2 Hydrophilicity of TiO_2-nanotubes surface

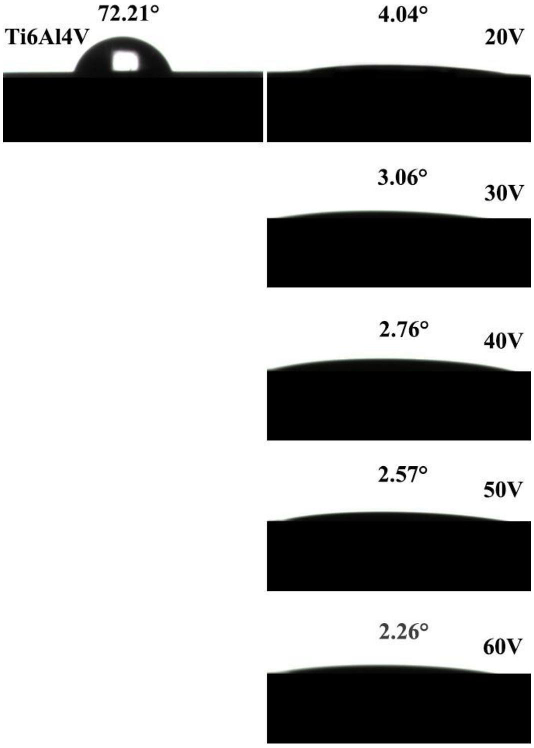

Figure 7. Contact angles of Ti6Al4V foil and TiO_2-nanotubes array anodized in the electrolyte containing EG, 0.25wt% NH_4F, and 4.0wt% H_2O for 3h.

Figure 7 shows the contact angle of Ti6Al4V and TiO_2-nanotubes film anodized in the electrolyte containing EG, 0.25wt% NH_4F, and 4 wt% H_2O content at 20V, 30V, 40V, 50V, and 60Vfor 3h, respectively. The Ti6Al4V alloy shows a hydrophobic surface with a contact angle of 72.21°. After anodization, the surface with TiO_2-nanotubes film becomes hydrophilic because the contact angle decreases to be smaller than that of Ti6Al4V surface. By determining the wettability of TiO_2-nanotubes surface anodized at 20V, 30V, 40V, 50V and 60V, the contact angle changes from 4.04° (20V) to 2.76° (40V), and then to 2.26° (60V). A study reported that the anodized TiO_2-nanoubular surfaces are transformed to hydrophilic surfaces regardless of anodization conditions [5]. This means that the anodization can change the surface wettability of the alloy and the film of TiO_2 nanotubes shows the good hydrophilicity. At high voltage, the diameter of TiO_2 nanotubes is large, and the contact angle is small. This indicates that the hydrophilicity of TiO_2-nanotubes film is enhanced with the increase of anodizing voltage.

4. CONCLUSIONS

Based on the method of orthogonal design of experiments (DOE), the highly-ordered TiO_2 nanotube arrays was successfully fabricated in EG electrolyte containing 0.25 wt% NH_4F. The morphology of TiO_2 nanotube arrays was characterized by SEM. The nanoporous layer, the nanograss, the bundled top parts, the ripples on the wall of tubes, and the serious collapse and disintegrate of the top part of TiO_2 nanotubes were observed on Ti6Al4V alloy. The long neat nanotube with honeycomb-like structure was also formed and arranged in an array. The statistical analysis indicated that the anodizing voltage was the primary factor in fabricating the dimension of the TiO_2 nanotubes. The voltage was linearly correlated with the diameter of anodized TiO_2 nanotubes. The optimal level for the water content and duration time was 4 wt% H_2O and 3h, respectively. The contact angle measurements revealed the surface wettability of Ti6Al4V alloy was hydrophilic and enhanced with the anodizing voltage increasing.

ACKNOWLEDGEMENTS

This work is financially supported by the China Scholarship Council (CSC) for State Scholarship Fund No. [2014]3012, National Natural Science Foundation of China (3127008, 11120101001, 61227902). the 111 Project (B13003), International Joint Research Center of Aerospace Biotechnology and Medical Engineering, Ministry of Science and Technology of China, Specialized Research Fund for the Doctoral Program of Higher Education, and National High Technology Research and Development Program of China (863 program, 2011AA02A102).

References

1. M.A. Hossain, J. Park, J.Y. Ahn, C. Park, Y. Kim, S.H. Kim, D. Lee, *Electrochim Acta*, 173 (2015) 665-671.
2. Q. Gui, Z. Xu, H. Zhang, C. Cheng, X. Zhu, M. Yin, Y. Song, L. Lu, X. Chen, D. Li, Acs *Appl Mater Inter*, 6 (2014) 17053-17058.
3. D. Losic, M.S. Aw, A. Santos, K. Gulati, M. Bariana, *Expert Opin Drug Deliv*, 12 (2014) 103-127.
4. A. Agarwal, T.L. Weis, M.J. Schurr, N.G. Faith, C.J. Czuprynski, J.F. McAnulty, C.J. Murphy, N.L. Abbott, *Biomaterials*, 31 (2010) 680-690.
5. A. Hamlekhan, A. Butt, S. Patel, D. Royhman, C. Takoudis, C. Sukotjo, J. Yuan, G. Jursich, M.T. Mathew, W. Hendrickson, A. Virdi, T. Shokuhfar, *Plos One*, 9 (2014) e96213.
6. S. Minagar, J. Wang, C.C. Berndt, E.P. Ivanova, C. Wen, *J Biomed Mater Res A*, 101 (2013) 2726-2739.
7. D. Regonini, C.R. Bowen, A. Jaroenworaluck, R. Stevens, *Mat Sci Eng R*, 74 (2013) 377-406.
8. F. Shen, Y. Zhu, X. Li, R. Luo, Q. Tu, J. Wang, N. Huang, *Appl Surf Sci*, 349 (2015) 589-598.
9. V. Zwilling, E. Darque-Ceretti, A. Boutry-Forveille, D. David, M.Y. Perrin, M. Aucouturier, *Surf Interface Anal*, 27 (1999) 629-637.
10. P. Roy, S. Berger, P. Schmuki, *Angew Chem Int Edit*, 50 (2011) 2904-2939.
11. H. Li, J.-W. Cheng, S. Shu, J. Zhang, L. Zheng, C.K. Tsang, H. Cheng, F. Liang, S.-T. Lee, Y.Y. Li, *Small*, 9 (2013) 37-44.
12. Y. Yang, X. Wang, L. Li, *Mater Sci Eng B*, 149 (2008) 58-62.
13. D. Gong, C.A. Grimes, O.K. Varghese, W.C. Hu, R.S. Singh, Z. Chen, E.C. Dickey, *J Mater Res*, 16 (2001) 3331-3334.
14. S. Berger, R. Hahn, P. Roy, P. Schmuki, *Phys Status Solidi* B, 247 (2010) 2424-2435.
15. Z. Lockman, S. Sreekantan, S. Ismail, L. Schmidt-Mende, J.L. MacManus-Driscoll, *J Alloys Compd*, 503 (2010) 359-364.
16. J.M. Macak, H. Tsuchiya, P. Schmuki, *Angew Chem Int Edit*, 44 (2005) 2100-2102.
17. K. Lee, A. Mazare, P. Schmuki, *Chem Rev*, 114 (2014) 9385-9454.

18. S.J. Garcia-Vergara, P. Skeldon, G.E. Thompson, H. Habazaki, *Electrochim Acta*, 52 (2006) 681-687.
19. J.E. Houser, K.R. Hebert, *Nat Mater*, 8 (2009) 415-420.
20. X. Zhu, L. Liu, Y. Song, H. Jia, H. Yu, X. Xiao, X. Yang, *Mater Lett*, 62 (2008) 4038-4040.
21. B. Chong, D.L. Yu, M.Q. Gao, H.W. Fan, C.Y. Yang, W.H. Ma, S.Y. Zhang, X.F. Zhu, *J Electrochem Soc*, 162 (2015) H244-H250.
22. S.Y. Zhang, D.H. Yua, D.D. Li, Y. Song, J.F. Che, S.Y. You, X.F. Zhua, *J Electrochem Soc*, 161 (2014) E135-E141.
23. Q.F. Gui, D.L. Yu, D.D. Li, Y. Song, X.F. Zhu, L. Cao, S.Y. Zhang, W.H. Ma, S.Y. You, *Appl Surf Sci*, 314 (2014) 505-509.
24. J.H. Lim, J. Choi, *Small*, 3 (2007) 1504-1507.
25. J. Naduvath, P. Bhargava, S. Mallick, *Chem Phys Lett*, 626 (2015) 15-19.
26. Y.Y. Song, R. Lynch, D. Kim, P. Roy, P. Schmuki, *Electrochem Solid St*, 12 (2009) C17-C20.
27. A. Valota, D.J. LeClere, P. Skeldon, M. Curioni, T. Hashimoto, S. Berger, J. Kunze, P. Schmuki, G.E. Thompson, *Electrochim Acta*, 54 (2009) 4321-4327.
28. S. Berger, J. Kunze, P. Schmuki, A.T. Valota, D.J. LeClere, P. Skeldon, G.E. Thompson, *J Electrochem Soc*, 157 (2010) C18-C23.
29. Y. Zhang, D. Yu, M. Gao, D. Li, Y. Song, R. Jin, W. Ma, X. Zhu, *Electrochim Acta*, 160 (2015) 33-42.
30. J.H. Xing, Z.B. Xia, J.F. Hu, Y.H. Zhang, L. Zhong, *Corros Sci*, 75 (2013) 212-219.